DOI: 10.13009/EUCASS2025-202
11TH EUROPEAN CONFERENCE FOR AERONAUTICS AND SPACE SCIENCES (EUCASS)

Performance analysis of a megawatt fuel cell-based electric powertrain for regional aircraft

K. Sommer, B. Ni*, J. Weiss*, O. Thalau* and C. Bänsch*†*
** German Aerospace Center (DLR), Institute of Engineering Thermodynamics*
Pfaffenwaldring 38-40, 70569 Stuttgart, Germany
cornelie.baensch@dlr.de
† Corresponding Author

Abstract
In this work, the performance of a hydrogen-electric powertrain for regional aircraft is analysed. The analysis is based on experimental and modelling results of the DLR-owned ground-based BALIS powertrain with up to 1.2 MW maximum power output consisting of an LH2 tank with a storage capacity of 200 kg, a fuel cell system of 12 polymer electrolyte membrane fuel cell modules in a 2s6p configuration, and an e-drive system of two permanent magnet synchronous machines connected mechanically with a summation gear. The results indicate that the subsystems work properly and substantiate the feasibility of LH2/PEMFC electric powertrains in the MW range.

1. Introduction

Hydrogen-electric propulsion is discussed as one option for the decarbonization of short-range and regional aircraft [1-3]. The application of polymer electrolyte membrane fuel cells (PEMFC) with liquid hydrogen (LH2) storage combines the high gravimetric energy density of hydrogen with high chain efficiencies [1, 2]. While the technology has already been demonstrated in flight in various projects mainly in the CS-23 class [4-8], the scale-up of such propulsion systems to the megawatt range is still subject of current research [9, 10]. Demonstrations relevant for CS-25 class have been reported by Airbus [11], who tested a combined PEMFC/e-drive unit on ground, and by Universal Hydrogen [8] carrying out a flight test with a Dash-8 aircraft, in which one conventional propulsion unit was replaced by a PEMFC-based electric powertrain. However, no scientific evaluation of these tests is available in literature.
From a technological perspective, one of the main barriers for the implementation of LH2/FC-based propulsion systems in the CS-25 class are the relatively low volumetric and gravimetric power densities as well as the volumetric energy density, which still lag significantly behind the corresponding combustion-based technologies. Furthermore, technology maturity and durability of fuel cells with the focus on reliable operation and robustness are still an issue, requiring intensive research and development. [8, 12-14]
Hence, to contribute to closing the knowledge gap about operability and performance capabilities of MW fuel cell-based powertrains for aviation the BALIS test environment has been developed at the German Aerospace Center (DLR) [15, 16]. In this work, a first analysis of the performance of the first-generation powertrain, based on experimental results gained in the e-motor and fuel cell test field as well as on simulation data from the validated model of the coupled liquid hydrogen/fuel cell system is given. Focus is on investigating the functionality and operational stability in the relevant parameter ranges.

2. BALIS system overview

2.1 Test facility

The DLR BALIS test environment is a modular, containerized test infrastructure for the investigation of fuel cell-based powertrains in the MW range. It is located at Innovation Campus in Empfingen, Germany. A picture of the test environment is shown in Figure 1. The test environment is divided into different test fields, which enable the experimental investigation of the powertrain subsystems e-drive, fuel cell system, battery and liquid hydrogen tank system. The test fields can be operated separately or combined in various coupling modes (“use cases”). The focus is on functionality tests with the flexibility to integrate different components and test systems (units under test, UUT) and to examine them in combination. After being built in the years 2022-2024, the test fields fuel cell and e-drive are

DOI: 10.13009/EUCASS2025-202

in operation, while the liquid hydrogen test field is still under development. A detailed explanation of the methodological approach and an overview of the different use cases are given in refs. [15, 16].

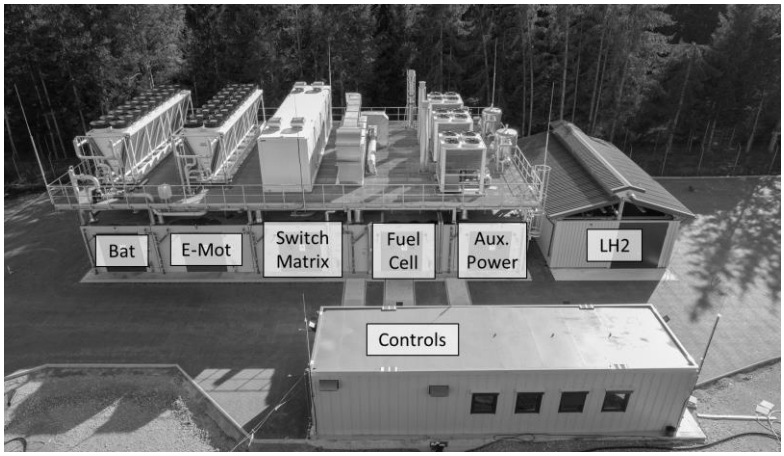

Figure 1: Aerial view of the DLR test environment BALIS, with the designation of the different test fields; “Bat”: Battery test field; “E-Mot”: E-motor test field; “Switch matrix”: Container for HV infrastructure with so-called switch matrix and DC-source/sinks; “Fuel Cell”: Fuel cell test field; “Aux. Power”: Container with power distribution devices for auxiliary power supply for the fuel cell system and test field monitoring; “LH2”: Liquid hydrogen tank test field; “Controls”: Control room.

2.2 First-generation powertrain

A first-generation powertrain system has been developed to be integrated and tested in the test environment. The system is based on commercial off-the-shelf components and modules, which do not fully meet aviation requirements. The aim is to establish an initial ground-based benchmark system to gain experimental data and identify technological gaps in the operation of MW hydrogen-electric propulsion systems. The first-generation fuel cell and e-drive system already have been integrated into the respective test fields and are put into operation. The LH2 tank system including evaporator is developed, while an integration into the LH2 test field is still pending. In a stepwise approach, the subsystems of the powertrain are investigated in different experimental and modelling studies, which are described in the following two sections.

3. Experimental

3.1 Set-up

Experimental studies were carried out in the e-motor and fuel cell test field focussing on the stationary performance under part and maximum load conditions. The goal was the characterization of the system performance and the proof of functionality of the system concept. The system principle is described in ref. [16]. Hence, only a brief overview of the test system applied in this work is given here.

HV infrastructure. The high voltage (HV) system of the facility enables the HV connection of the different test fields and load simulation. Centrepiece of the HV system is the switch matrix, which allows the connection of the whole HV system in flexible use cases. In this work, load simulation in each experiment is realized with two bidirectional DC source/sinks (AVL, 1250 A / 825 kW) exchanging required or surplus energy with the grid via a transformer. The respective switching points of the switch matrix are connected to two power distribution units (PDU, AVL, 1200 V / 1250 A (output current), 750 kW) in each test field. The HV interfaces of the UUTs are connected to the respective PDU. For fuel cell MW testing the “partly parallel” use case is applied, while E-drive testing was carried out in the “full parallel” use case. An overview over the HV wiring concept of the applied use cases for the MW proof of performance tests is given in Figure 2.

DOI: 10.13009/EUCASS2025-202

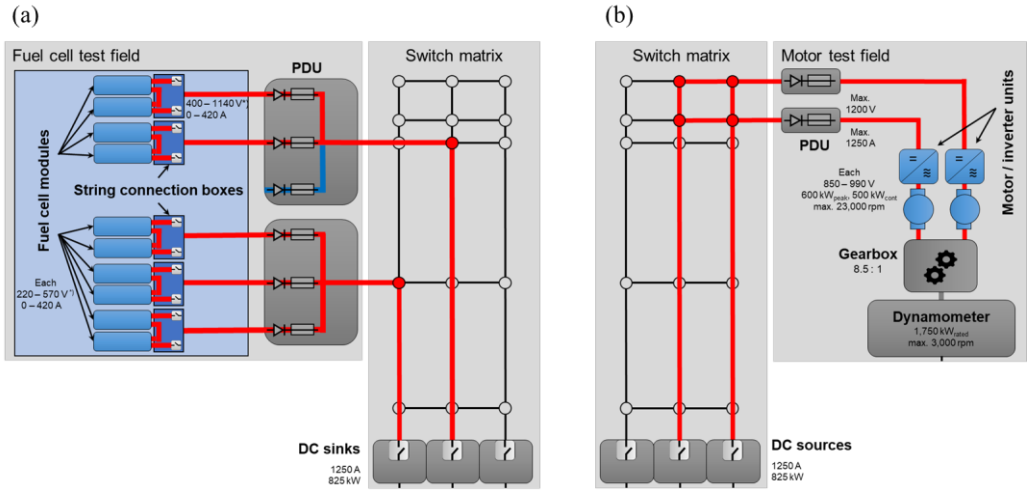

Figure 2: Schematic of test set-ups applied in the MW proof of performance tests: (a) fuel cell system set-up, (b) e-drive set-up; grey: infrastructure, blue: UUTs; red lines indicate the active part of the HV system applied in the respective MW proof of performance tests; *) theoretical max. voltage.

Fuel cell system. The multi stack fuel cell system (MFCS) consists of 12 commercial fuel cell modules (PS-100, PowerCell, P_{gross} = 120 kW, P_{net} = 100 kW, I_{max} = 420 A) in a configuration with pairs of fuel cell modules in series ("fuel cell string") and six fuel cell strings connected in parallel (denotation: 2s6p). For the current analysis 10 modules (5 serial master/slave module strings, 2s5p) are used. Two and three fuel cell strings, respectively, are connected in a direct parallel configuration via the test field PDUs. No DCDC converter is implemented in this MFCS, therefore active control of the voltage levels of the different strings is not possible. The MFCS is controlled in current following mode. In this control approach, the target current is set by the user and measured by the HV infrastructure. Balance-of-plant components of the MFCS are controlled by the respective built-in controllers of the individual modules, according to the actual drawn current. At the beginning of the test campaign, the string characterization was achieved by recording polarization curves in uniform procedures, which ensure stationary conditions. For this characterization each string was operated individually via the corresponding PDU, while the other strings remained switched off. The subsequent test run of the whole 2s5p fuel cell system was carried out in "full parallel" configuration with the PDUs galvanically connected via the switch matrix. For both, string characterization and "full parallel" tests the maximum string output was limited to 400 A in order to avoid exceeding the current limit of the PDU. Subsequently, tests in "partly parallel" configuration were carried out (cf. Figure 2). During these tests the string current limit was adjusted manually in order to achieve the MW proof of performance while respecting the different current limits of the devices. A detailed description of the characterization procedures is given in ref. [17].

E-drive system. The e-drive system is composed of two permanent magnet synchronous machines with inverter (Compact Dynamics, 600 kW_{max}/500 $kW_{contiuous}$ @ 17,000 rpm), which are connected mechanically in a parallel configuration via summation gear (Chemnitzer Zahnradfabrik, >98% efficiency). Each machine is powered by one test field PDU. Vibrations are detected with a 3D acceleration sensor (Ibis, AE 100.303), which is placed in the top of the gearbox.

3.2 Results and discussion

Fuel cell system. Focus of the performance analysis in this work is put on the maximum power output of the MFCS. For a detailed analysis of the experimental results, the reader is referred to ref. [17]. In the characterization tests of the individual fuel cell strings, significant differences in performance were observed between the strings. The maximum string power $P_{n,max}$ at 400 A varied from 208 to 224 kW.

Tests of the 2s5p fuel cell system in the "full parallel" configuration resulted in a maximum power $P_{fp,max}$ of 926 kW. The theoretical maximum power of the 2s5p $P_{th,max}$ was calculated based on:

$$P_{th,max} = \sum_{n=1}^{5} U_{n,400A} \cdot 400\ \text{A}\,, \qquad \textbf{(1)}$$

DOI: 10.13009/EUCASS2025-202

with $U_{n,400A}$ being the voltage of string number n at 400 A output current. A value of 1069 kW was obtained. Hence, $P_{fp,max}$ is 86 % below $P_{th,max}$. This deviation results from the direct parallel connection of the strings via one bus bar, which forces all strings to be operated at the same bus voltage. As soon as the best performing string reaches the upper string current limit of 400 A, the overall power output cannot be increased further and the voltage of all strings is determined by the voltage level of the best performing string at its current limit. However, the other strings cannot deliver the limit current at this voltage and the overall system power is reduced compared to the theoretical value. If the performance differences of the individual strings increase during the system's lifetime, the deviation of $P_{fp,max}$ from $P_{th,max}$ further increases. From this perspective, a beneficial control approach may be to turn off the strings that show poorer performance in part load scenarios, while only applying the strings that show better performance. This leads to an accelerated aging of the better performing strings, keeping the differences in performance as small as possible.

Sophisticated design approaches of MFCS consider the integration of DCDC converters for individual control of the voltage level of the parallel connected stacks, while increasing system mass and complexity (see e.g. refs. [18,19]). This approach is envisioned to be implemented in the BALIS system in the future, comparing the advantages and disadvantages of the different approaches for aircraft applications. In order to achieve a first validation of this approach and to increase the maximum power level of the system, the system was operated in the "partly parallel" configuration. In this use case the different PDUs are operated galvanically isolated while the current request refers to the whole system. This allows to control the voltage at the PDU buses separately simulating the effect of an integration of two DCDC converter modules on the system output. The measuring results of this test run are shown in Figure 3. At a system current of 1719 A the respective best performing string of each part of the system reached the string current limit of 400 A. A power output $P_{pp,max}$ of 966 kW was obtained, which is 40 kW higher than $P_{fp,max}$ and 90 % below $P_{th,max}$. The current request was further increased in smaller steps with short duration to approach the maximum system power limit. For the MW proof of performance, the string current limit was increased to 420 A, while monitoring the PDU current limit of 1250 A simultaneously. A power output of 1020 kW and with that the MW proof of performance of the UUT was achieved. However, stationary conditions could not be reached at a power above 1 MW and the system had to be shut down after 120 s to prevent from overheating. While a detailed discussion of this observation is beyond the scope of the present work, an optimization of the multi-stack cooling system is assumed to improve this non-optimal system behaviour and ensure a stable system cooling at maximum power.

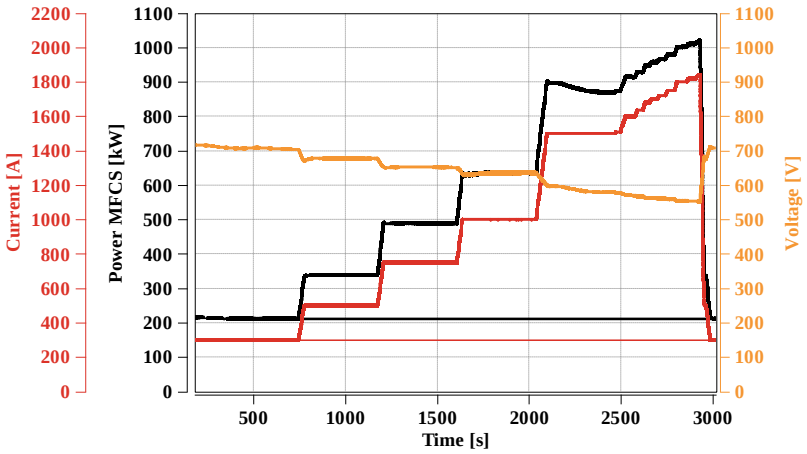

Figure 3: Current and voltage measured over time and corresponding calculated power output of the fuel cell system in the "partly parallel" configuration.

Simultaneously, the performance data of the individual strings was characterized during the "full parallel" and "partly parallel" test runs. An oscillation over time of the string power values was observed, while the system voltage reached stationary conditions. This behaviour was observed at all power levels with different periodic times and amplitudes. However, these oscillations never led to a system instability or shutdown. A detailed analysis of the string behaviour during the test runs is given in ref. [17].

E-drive system. Focus of the first e-drive test campaign was the proof of performance at maximum power level. The electric motors first were operated in single-mode operation. Maximum peak electrical power of 600 kW at 17,000 rpm for ten minutes and continuous electrical power of 500 kW were achieved in single-mode operation according to the specifications of the manufacturer. However, several performance limitations were observed:

1. A motor defect occurred and impurities in the cooling loop were assumed to be the cause. As a result, the limit for the maximum particle size in the cooling circuit was reduced to 50 µm. Filters were adapted accordingly and the cooling circuit was redesigned in order to be able to handle the increased pressure drop

DOI: 10.13009/EUCASS2025-202

due to the adapted filters. Frequent chemical analysis of the cooling fluid composition and exchange of the cooling fluid may be necessary to prevent from further system failure.

2. Pronounced torque oscillations were observed during single-mode operation. While a detailed investigation of the cause is beyond the scope of this paper, future work should focus on optimizing the mechanical behaviour and reducing torque fluctuations in order to reduce the mechanical stress on the system.

The measuring results of the tests in dual-mode operation at a total input current between 1,040 and 1,360 A are shown in Figure 4. At the operational limit of 600 kW electrical power at each inverter input and 1,200 kW in total, a maximum mechanical power output of 1,140 kW at the dynamometer shaft and a system efficiency of 95 % was obtained at a rotational speed of 15,000 rpm. Hence, the MW proof of performance of the UUT was achieved. However, also in dual-mode operation pronounced torque oscillations were observed. In addition, significant vibrations were characterized with the acceleration sensor on the top of the gearbox, with values along the three axes between 2 and 6 mm s^{-1} depending on the axis and power level.

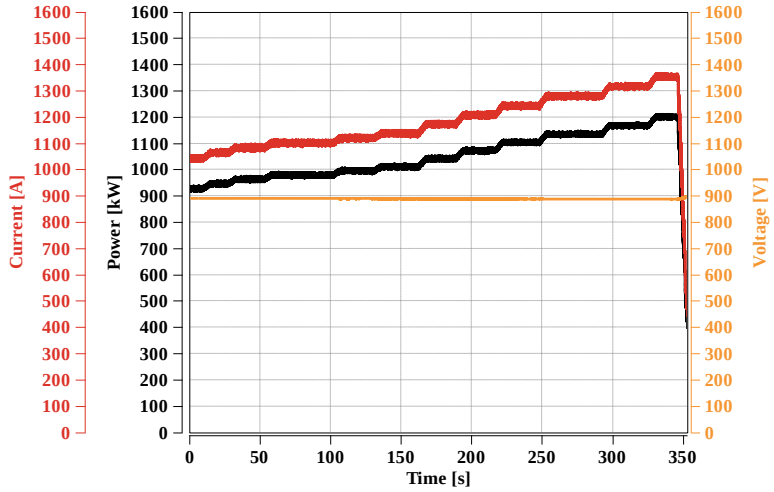

Figure 4: Current and voltage measured over time and corresponding calculated power input of the e-drive system in the dual-mode operation during the test run for MW proof of performance at 15,000 rpm.

In further test runs, an attempt was made to characterize the entire characteristic map of the e-drive system in dual-mode operation. However, after small positive and negative deviations from a speed of 15,000 rpm, the vibrations exceeded the limit of 7 mm $s^{-1}$and the tests had to be stopped. Consequently, the mechanical instabilities currently limit the operability of the UUT. However, while the cause of the instabilities is not yet found, it seems probable that the reason lies in the mechanical design of the test stand. Further tests have to be carried out to investigate the cause of the instabilities. Furthermore, the adjustment of the gearbox and dynamometer shaft as well as the dynamometer calibration has to be improved.

4. Simulation

3.1 Modelling approach

Goal of the simulation work is the investigation of the behaviour of the hydrogen supply to the fuel cell system from the liquid hydrogen tank under dynamic load scenarios. An in-house model is developed in Modelica which includes the tank, the hydrogen conditioning, the multi-modular fuel cell system, and the cooling system. Dissipated heat from the fuel cell is used to evaporate and preheat the hydrogen before supplying it to the fuel cell system. An electrical heater is integrated to provide additional heat during start-up if the cooling fluid is too cold. The fuel cell system consists of several fuel cell modules similar to the configuration in the BALIS fuel cell system described above. The higher the number of implemented fuel cell modules the higher the computational effort. As a compromise a 2s3p configuration was selected for the modelling study. The fuel cell module model includes a 0D stack model, and the balance-of-plant subsystems for cathode, anode and cooling. Neither degradation nor performance differences were considered in the model. The modelling approach is described in detail in ref. [20].

DOI: 10.13009/EUCASS2025-202

3.2 Model validation

The fuel cell model is validated at the stack and system levels. Stack validation is carried out using experimental literature data from ref. [21] at varying cathode humidities (CRH) and anode humidities (ARH). A comparison of simulation and literature data is shown in Figure 5. A good agreement of simulated and literature data is observed for high cathode humidities with a mean absolute percentage error (MAPE) above 5.3 % for CRH > 50 %. In contrast, at lower CRH levels the simulated values deviated significantly from the literature data. This deviation is assumed to result from inhomogeneities of the membrane humidification under dry conditions [22], which cannot be depicted by the 0D stack model. Overall, it can be concluded that the stack model is valid for operational ranges with high membrane humidification. The restriction that dry conditions cannot be captured accordingly is acceptable for the application area of the model, as sufficient humidification must be ensured in normal operation for aircraft application.

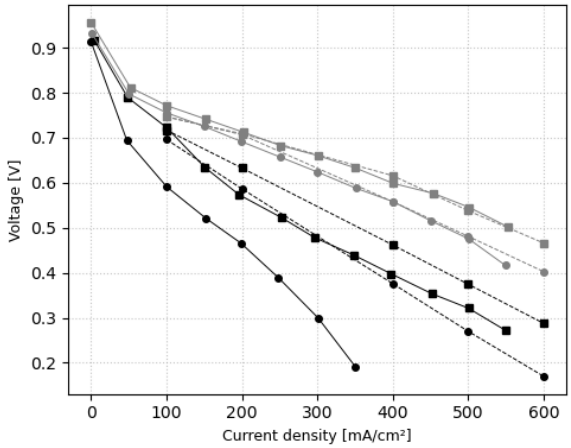

Figure 5: Comparison of simulated polarization curves with experimental stack data from ref. [21] at different values for cathode humidity (CRH) and anode humidity (ARH); dotted lines: simulation, solid lines: experiment; black: CRH = 10 %, grey CRH = 100 %; dots: ARH = 60 %, squares: ARH = 90%.

Fuel cell model validation on system level is achieved by the comparison with experimental data of BALIS fuel cell string tests, which is shown in Figure 6. A good agreement between the simulation and experimental data was observed for low power levels and stationary conditions with an MAPE of 3.3 %. At high power levels an overshoot of the voltage was observed in the experiments. It is assumed to result from increased response time of the air supply, which is not depicted in the model. However, as the simulation aims to investigate the hydrogen supply, the representation of the air supply is simplified and we assume that this limitation will not significantly affect the accuracy of the hydrogen supply description.

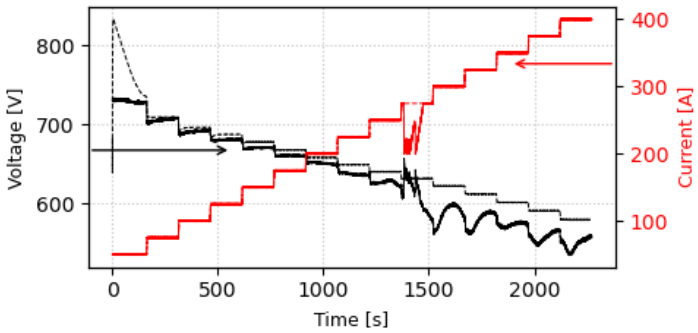

Figure 6: Comparison of simulated values of voltage and current over time and experimental data of the BALIS fuel cell system; dotted lines: simulation, solid lines: experiment.

In addition to the current and voltage, the simulated hydrogen mass flow rate of the fuel cell module was compared to experimental data of the BALIS fuel cell system. An MAPE of 16 % was obtained, which is assumed to lie within an acceptable range for system simulation.
Due to lack of data a validation of the liquid hydrogen tank system is still pending.

DOI: 10.13009/EUCASS2025-202

3.3 Results and discussion

A generic load profile was assumed to represent the load conditions in different flight phases. Heat flows, and hydrogen supply pressure and temperature, as well as stack operating conditions were simulated during this load profile. An overview of the obtained heat flows is given in Figure 7. During start-up the electrical heater with a power of 60 kW keeps the cooling fluid at the required minimum temperature of 35°C. In total, 1.4 kWh of electrical energy is required by the electrical heater indicating that the amount of energy in addition to the waste heat of the fuel cell system is very small. In general, the heat dissipated from the fuel cell system is roughly an order of magnitude higher than the heat consumed for hydrogen conditioning for all flight phases. These results suggest that the heat losses from the fuel cell system are sufficient to supply the heat required for hydrogen conditioning. However, despite the fact that the hydrogen conditioning represents a significant heat sink, a large amount of low temperature heat still has to be released into the environment by the aircraft's cooling system.

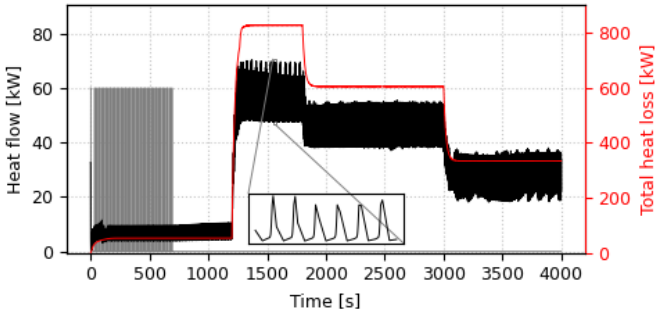

Figure 7: Simulated heat flows during the assumed load profile; grey: heat flow from electrical heater, black: heat flow for LH2 evaporation/heating, red: total flow of dissipated heat from fuel cell modules; Note, that the total heat loss of the fuel cell system is roughly an order of magnitude higher than the heat required for hydrogen conditioning.

Resulting hydrogen temperatures and pressures at the anode inlet during the flight phases are shown in Figure 8. Ranging from 10 to 40 °C over the flight mission the hydrogen inlet temperature always meets the requirement above the minimum value of 5 °C. The anode inlet pressure follows the respective setpoints during all flight phases. Fluctuations in the inlet pressure are observed due to anode purging. However, these fluctuations stay within an acceptable range of 300 mbar, which is in line with the observations of Wang *et al.* [23]. A detailed discussion of the findings is given in ref. [20].

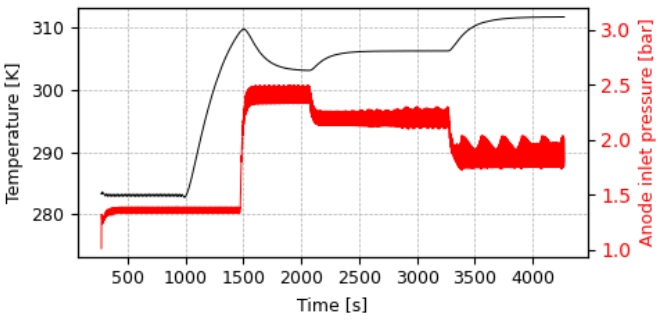

Figure 8: Simulated hydrogen supply temperature (black) and anode inlet pressure (red) during the assumed load profile.

Overall, the modelling results suggest that the LH2 system is designed properly to supply the fuel cell system with hydrogen under the required conditions. Minimal influences of the hydrogen supply from the LH2 system on the fuel cell performance is expected.

4. Weight analysis

The powertrain mass is one critical issue, when evaluating the suitability for aircraft application. However, the design focus of the BALIS first-generation powertrain lay on the system functionality, while system weight was considered as requirement with lower priority yet. A brief analysis has been carried out in order to document the weight status as

DOI: 10.13009/EUCASS2025-202

a first benchmark. An overview of specific power densities for e-drive and fuel cell system as well as gravimetic index for LH2 tank system is given in Table 1. The specific power density of the BALIS fuel cell system is in line with the typical power densities in automotive applications [3]. With the push towards hydrogen-electric aviation, significant improvements of fuel cell specific power on system level for aircraft applications have been reported in recent years e.g. by ZeroAvia [24] and Intelligent Energy [25]. Improvements can be made on the basis of compact system design, light-weight components, increased stack specific power and combination of balance-of-plant components in MFCS. The BALIS e-drive technology already exceeds the state-of-the-art values reported in ref. [26]. However, one must have in mind that the high-speed motors require a transmission gear to achive the target rotational speed ranges of a propeller, which also accounts to the system weight. The BALIS tank gravimetric efficiency is poor compared to the state-of-the-art and target values [27]. The main reason for the poor gravimetric performance is that the refuelling unit is integrated into the BALIS tank system and contributs to the system mass. In addition, the tank is made of stainless steel, which is the most mature but also heavy technology for LH2 tank fabrication. Aircraft relevant tank design should consider an external ground support unit for tank refuelling and lightweight materials such as aluminium and composite materials.

Table 1: Overview of specific power density of the fuel cell and e-drive system and the gravimetric efficiency of the tank system in comparison to state-of-the-art and target values from literature.

	BALIS system	**State of the art**	**Target**
Fuel cell system specific power density [kW/kg]	0.5	0.5-2.1 [3, 24]	1.5-2 [27]
E-drive specific power density [kW/kg]	13.2 (cont. power; excl. gear)	~8 [26]	20 [26]
LH2 tank gravimetric efficiency [%]	6.8	7.5 [3] – 20 [27]	35-38 [27]

5. Conclusion

Based on the performance analysis carried out in this work several conclusions can be drawn:

1. Stable operation of a MFCS in a serial/parallel configuration without converter is possible up to MW power output. The stable provision of stack cooling power is still a challenge, which should be tackled by developing sophisticated efficient, robust and light-weight cooling approaches for high-power MFCS.
2. Due to the direct parallel configuration of the MFCS, power losses of 13 % compared to the theoretical maximum power were observed. In addition, current oscillations between the fuel cell strings occurred. These effects can be eliminated by integrating a DCDC converter system, although increasing system weight and complexity.
3. Stable operation of the e-drive system in the dual-mode operation is possible with MW power output. Mechanical instabilities, namely torque oscillations and vibrations, are a challenge varying strongly dependent on the rotational speed. However, the mechanical design and installation of the e-motor test stand has to be adjusted and refined before any conclusions regarding performance limitations of the UUT can be drawn.
4. The simulation results suggest that stable operation of the coupled LH2/fuel cell system is possible under flight-relevant load profiles. An additional electric heater is required for cold start conditions, but the amount of required power and energy is relatively small compared to the system size and power.
5. Hydrogen conditioning can serve as a relevant heat sink with a heat demand of roughly 10 % of the heat dissipated by the fuel cell system. Nevertheless, fuel cell cooling remains a main challenge for hydrogen-electric aircraft as the surplus of low-temperature heat is still high.
6. Although not being the prioritized requirement of the BALIS system design, the UUTs' system masses in general are close to the best-case limit of the state-of-the-art technology. While the e-drive system already exhibits outstanding specific power values, focus of mass reduction measures should be put on the fuel cell and LH2 tank system. In more comprehensive weight analyses, the aircraft integration including the cooling system should be considered.

DOI: 10.13009/EUCASS2025-202

Acknowledgement

This work was supported by the Federal Ministry of Digital and Transport of Germany as part of the National Hydrogen and Fuel Cell Technology Innovation Program (NIP) (research project BALIS 2.0, 03B10708C) and the Federal Ministry for Economic Affairs and Energy as part of the LuFo VI-3 Program (research project 328H2-FC, 20M2109A). The authors thank their colleagues Marco Richter, Andreas Gienger, and Timo Braun for their technical and test support. The support of the project teams of AVL, Power Cell, Compact Dynamics, and Air Liquide advanced Technologies is gratefully acknowledged.

References

[1] Baroutaji, A., Wilberforce, T., Ramadan, M., Olabi, A. G. 2019. Comprehensive investigation on hydrogen and fuel cell technology in the aviation and aerospace sectors. *Renew. Sustain. Energy Rev.* 106:31-40.

[2] Dahal, K., Brynolf, S., Xisto, C., Hansson, J., Grahn, M., Grönstedt, T., and Lehtveer, M. 2021. Techno-economic review of alternative fuels and propulsion systems for the aviation sector. *Renew. Sustain. Energy Rev.* 151:111564.

[3] Tiwari, S., Pekris, M. J., and Doherty, J. J. 2024. A review of liquid hydrogen aircraft and propulsion technologies. *Int. J. Hydrog. Energy* 57:1174-7796.

[4] Lapeña-Rey, N., Mosquera, J., Bataller, E., and Ortí, F. 2010. First Fuel-Cell Manned Aircraft. *J. Aircraft* 47:1825-1835.

[5] Romeo, G., Boello, F., Correa, G., and Cestino, E. 2013. ENFICA-FC: Design of transport aircraft powered by fuel cell & flight test of zero emission 2-seater aircraft powered by fuel cells fueled by hydrogen. *Int. J. Hydrog. Energy* 38:469-479.

[6] H2Fly. 2023. World's First Flight of Liquid Hydrogen Aircraft. Press Release, Stuttgart, Germany & Maribor, Slovenia.

[7] ZeroAvia. 2023. ZeroAvia Successfully Completes Initial Dornier 228 Flight Test Campaign. Press Release, Kemble, United Kingdom & Hollister, USA.

[8] UniversalHydrogen. 2023. Universal Hydrogen Successfully Completes First Flight of Hydrogen Regional Airliner. Press Release, Los Angeles & Moses Lake, USA.

[9] Hartmann, C., Nøland, J. K., Nilssen, R., and Mellerud, R. 2022. Dual Use of Liquid Hydrogen in a Next-Generation PEMFC-Powered Regional Aircraft With Superconducting Propulsion. *IEEE Transactions on Transportation Electrification* 8:4760-4778.

[10] Schefer, H., Fauth, L., Kopp, T. H., Mallwitz, R., Friebe, J., and Kurrat, M., Discussion on Electric Power Supply Systems for All Electric Aircraft. *IEEE Access* 8:84188-84216.

[11] Airbus. 2024. First ZEROe engine fuel cell successfully powers on. Available from: https://www.airbus.com/en/newsroom/stories/2024-01-first-zeroe-engine-fuel-cell-successfully-powers-on (downloaded at 18 September 2024).

[12] Sharaf, O. Z., and Orhan, M. F. 2014. An overview of fuel cell technology: Fundamentals and applications. *Renew. Sustain. Energy Rev.* 32:810-853.

[13] Dincer, I., and Acar, C. 2016. A review on potential use of hydrogen in aviation applications. *Int. J. Sustain. Aviat.* 2: 74-100.

[14] Jamal, T., Shafiullah, G. M., Dawood, F., Kaur, A., Arif, M. T., Pugazhendhi, R., Elavarasan, R. M., and Ahmed, S. F. 2023. Fuelling the future: An in-depth review of recent trends, challenges and opportunities of hydrogen fuel cell for a sustainable hydrogen economy. *Energy Reports* 10:2103-2127.

[15] Fritz, J., Bänsch, C., Weiss, J., Hacker, G., Diarra, D., Bever, C., and Thiele, I. 2022. Systems Engineering Methodology on a Multi-Integration Test Environment for Fuel Cell Flight Propulsion Systems. Deutscher Luft- und Raumfahrtkongress, Deutsche Gesellschaft für Luft- und Raumfahrt - Lilienthal-Oberth e.V., Dresden, Germany.

[16] Weiss, J., Diarra, D., Sommer, K., Ni, B, Thalau, O., and Bänsch, C. 2024. Modular test environment for fuel cell-based electric powertrains for aviation: Methodological approach of the BALIS test fields fuel cell, battery, and e-drive. Deutscher Luft- und Raumfahrtkongress, Deutsche Gesellschaft für Luft- und Raumfahrt - Lilienthal-Oberth e.V., Hamburg, Germany.

[17] Sommer, K., Weiss, J., and Bänsch, C. 2025. Experimental investigation of the efficiency of a multi-stack fuel cell system for aviation applications in the megawatt range. 11th European Conference for AeroSpace Sciences, Rome, Italy.

[18] Marx, N., Boulon, L., Gustin, F., Hissel, D., and Agbossou, K. 2014. A review of multi-stack and modular fuel cell systems: Interests, application areas and on-going research activities. *Int. J. Hydrog. Energy* 39:12101-12111.

DOI: 10.13009/EUCASS2025-202

[19] Zhou, S., Fan, L., Zhang, G., Gao, J., Lu, Y., Zhao, P., Wen, C., Shi, L., and Hu, Z. 2022. A review on proton exchange membrane multi-stack fuel cell systems. *Appl. Energy* 310:118555.
[20] Ni, B., Weiss, J., and Bänsch, C. 2024. Simulation of hydrogen supply in coupled PEM fuel cell/LH2 tank systems under aviation-relevant conditions. Deutscher Luft- und Raumfahrtkongress, Deutsche Gesellschaft für Luft- und Raumfahrt - Lilienthal-Oberth e.V., Hamburg, Germany.
[21] Yan, Q., Toghiani, H., and Wu, J. 2006. Investigation of water transport through membrane in a PEM fuel cell by water balance experiments. *J. Power Sources* 158:316-325.
[22] Reshetenko, T. V., Bender, G., Bethune, K., and Rocheleau, R. 2012. Systematic studies of the gas humidification effects on spatial PEMFC performance distributions. *Electrochim. Acta* 69:220-229.
[23] Wang, Q., Li, J., Bu, Y., Xu, L., Ding, Y., Hu, Z., Liu, R., Xu, Y., and Qin, Z., 2020. Technical assessment and feasibility validation of liquid hydrogen storage and supply system for heavy-duty fuel cell truck. Proceedings of the 2020 4th CAA International Conference on Vehicular Control and Intelligence (CVCI), Hangzhou, China.
[24] ZeroAvia. 2025. SuperStack Flex Fuel Cell System, Datasheet, available from https://zeroavia.com/superstack-flex-brochure/#download-brochure (accessed on 27 Jan 2025)
[25] Intelligent Energy. 2025. IE-FLIGHT fuel cell systems enabling zero emission aviation, Datasheet, available from https://www.intelligent-energy.com/our-products/ie-flight/ (accessed on 27 Jan 2025).
[26] Bird, J. Z., 2022. A Review of Electric Aircraft Drivetrain Motor Technology. *IEEE Trans. Magn.* 58:1-8.
[27] Clean Sky 2, Joint Undertaking Fuel Cells and Hydrogen. 2020. Hydrogen-powered aviation: A fact-based study of hydrogen technology, economics, and climate impact by 2050, Report, Publications Office of the European Union, doi: 10.2843/471510.